


 Cite this: *RSC Adv.*, 2023, 13, 26475

# Engineering electronic structures and optical properties of a MoSi<sub>2</sub>N<sub>4</sub> monolayer *via* modulating surface hydrogen chemisorption†

 Yumei Zhang,<sup>a</sup> Shunhong Dong,<sup>a</sup> Pachaiyappan Murugan,<sup>a</sup> Ting Zhu,<sup>ID ab</sup>  
 Chen Qing,<sup>a</sup> Zhiyong Liu,<sup>\*ab</sup> Weibin Zhang<sup>\*ab</sup> and Hong-En Wang<sup>ID \*ab</sup>

Recently, a MoSi<sub>2</sub>N<sub>4</sub> monolayer has been successfully synthesized by a delicately designed chemical vapor deposition (CVD) method. It exhibits promising (opto)electronic properties due to a relatively narrow bandgap (~1.94 eV), high electron/hole mobility, and excellent thermal/chemical stability. Currently, much effort is being devoted to further improving its properties through engineering defects or constructing nanocomposites (e.g., van der Waals heterostructures). Herein, we report a theoretical investigation on hydrogenation as an alternative surface functionalization approach to effectively manipulate its electronic structures and optical properties. The calculation results suggested that chemisorption of H atoms on the top of N atoms on MoSi<sub>2</sub>N<sub>4</sub> was energetically most favored. Upon H chemisorption, the band gap values gradually decreased from 1.89 eV (for intrinsic MoSi<sub>2</sub>N<sub>4</sub>) to 0 eV (for MoSi<sub>2</sub>N<sub>4</sub>-16H) and 0.25 eV (for MoSi<sub>2</sub>N<sub>4</sub>-32H), respectively. The results of optical properties studies revealed that a noticeable enhancement in light absorption intensity could be realized in the visible light range after the surface hydrogenation process. Specifically, full-hydrogenated MoSi<sub>2</sub>N<sub>4</sub> (MoSi<sub>2</sub>N<sub>4</sub>-32H) manifested a higher absorption coefficient than that of semi-hydrogenated MoSi<sub>2</sub>N<sub>4</sub> (MoSi<sub>2</sub>N<sub>4</sub>-16H) in the visible light range. This work can provide theoretical guidance for rational engineering of optical and optoelectronic properties of MoSi<sub>2</sub>N<sub>4</sub> monolayer materials *via* surface hydrogenation towards emerging applications in electronics, optoelectronics, photocatalysis, etc.

 Received 3rd July 2023  
 Accepted 29th August 2023

DOI: 10.1039/d3ra04428a

[rsc.li/rsc-advances](https://rsc.li/rsc-advances)

## 1. Introduction

In the past two decades, two-dimensional (2D) nanomaterials<sup>1–3</sup> have attracted enormous attention due to their unique physical and chemical properties, such as high surface area, fast migration of photo-induced electrons and holes to the reaction interface/front, high charge carrier separation efficiency, superior electronic and optical properties and rich reaction sites. Particularly, identification of two-dimensional layered materials in the monolayer limit can lead to the discovering of some new phenomena and unusual properties. Thus, researchers have continuously explored new 2D (monolayer) nanomaterials through experimental and theoretical investigations for various emerging applications in photoelectric and energy-intensive fields.

Recently, Ren's group successfully synthesized a new monolayered MoSi<sub>2</sub>N<sub>4</sub> material *via* a modified chemical vapor deposition (CVD) method.<sup>4</sup> The MoSi<sub>2</sub>N<sub>4</sub> monolayer was constructed by septuple atomic layers of Ni–Si–N–Mo–N–Si–N, as viewed as a MoN<sub>2</sub> layer sandwiched between two Si–N bilayers.<sup>5</sup> It displayed a bandgap of ~1.94 eV with a high mechanical strength and excellent chemical stability in atmosphere. These properties endowed MoSi<sub>2</sub>N<sub>4</sub> with promising applications in electronic/optoelectronic devices, optical sensors, and photocatalysis.

The great application potential of MoSi<sub>2</sub>N<sub>4</sub> monolayer material has spurred increasing interest in further improving its properties by constructing various (van der Waals) heterostructures. For example, Ang *et al.* reported tunable electronic properties and band alignments in MoSi<sub>2</sub>N<sub>4</sub>/GaN and MoSi<sub>2</sub>N<sub>4</sub>/ZnO van der Waals heterostructures.<sup>6</sup> Nguyen *et al.* studied the effects of interlayer coupling and under electric fields on the electronic structures of type-II C<sub>3</sub>N<sub>4</sub>/MoSi<sub>2</sub>N<sub>4</sub> heterostructure.<sup>7</sup> In addition, two-dimensional metal/semiconductor contact in a Janus MoSH/MoSi<sub>2</sub>N<sub>4</sub> van der Waals heterostructure<sup>8</sup> and MoSi<sub>2</sub>N<sub>4</sub>/MoS<sub>2</sub> van der Waals heterostructure with good optoelectronic performance and tunable electronic properties<sup>9</sup> were investigated. Apart from heterostructure engineering, Cui *et al.* found that metal atoms-adsorbed MoSi<sub>2</sub>N<sub>4</sub> (ref. 10) systems

<sup>a</sup>Yunnan Key Laboratory of Optoelectronic Information Technology, College of Physics and Electronic Information, Yunnan Normal University, Kunming 650500, China. E-mail: liuzhiyong@ynnu.edu.cn; 220001@ynnu.edu.cn; hongen.wang@outlook.com

<sup>b</sup>Key Laboratory of Advanced Technique & Preparation for Renewable Energy Materials, Ministry of Education, Yunnan Normal University, China

† Electronic supplementary information (ESI) available. See DOI: <https://doi.org/10.1039/d3ra04428a>



could enable the manufacture of spintronic and vacuum field emission nanodevices. Luo *et al.* used first principles calculations to study the structural and electronic properties of organic molecules-doped MoSi<sub>2</sub>N<sub>4</sub> monolayers,<sup>11</sup> demonstrating the importance of molecular doping in tuning the electronic properties of MoSi<sub>2</sub>N<sub>4</sub> with extended applications.

Heterostructure engineering,<sup>12,13</sup> adsorption and substitutional doping<sup>14–19</sup> have been proven to be effective ways to modify various properties of semiconductor materials. In addition, surface functionalization,<sup>20–24</sup> such as fluoridation and hydrogenation, can also be used to manipulate the properties of 2D materials. Recently, Binh *et al.* applied the hydrogenation method to change the properties of GeC,<sup>25</sup> and InN<sup>26</sup> monolayers, largely extending the applications of these materials. Chen *et al.* demonstrated that the fluorinated MoSi<sub>2</sub>N<sub>4</sub> monolayer<sup>27</sup> may exhibit a variety of properties and have the potential to fabricate novel optoelectronic devices by simply adjusting the degree of fluorination. Given the structure similarity between GeC/InN and MoSi<sub>2</sub>N<sub>4</sub>, hydrogenation could be a simple, clean, yet effective approach to engineer the electronic and optical properties of MoSi<sub>2</sub>N<sub>4</sub> monolayers and expand its applications.

In this work, we performed a comprehensive first-principles density functional theory study on the hydrogenation of MoSi<sub>2</sub>N<sub>4</sub> monolayer. The calculations reveal that the hydrogenated MoSi<sub>2</sub>N<sub>4</sub> monolayers are thermodynamically stable. Meantime, electronic structures and optical properties of hydrogenated MoSi<sub>2</sub>N<sub>4</sub> can be well regulated as a function of hydrogenation degree on the MoSi<sub>2</sub>N<sub>4</sub> surface. The simulation results suggest that the hydrogenated MoSi<sub>2</sub>N<sub>4</sub> monolayers can have promising applications in photocatalysis<sup>28</sup> and other clean energy-related fields.

## 2. Computational details

First-principles calculations based on quantum mechanics<sup>29</sup> can provide a reliable means to investigate the behavior of electrons and nuclei under specific circumstances. In current work, the electronic structure<sup>30</sup> and optical properties of both the pristine and hydrogenated MoSi<sub>2</sub>N<sub>4</sub> monolayers were studied. Based on density functional theory (DFT)<sup>31,32</sup> and plane-wave pseudo-potential basis, a collection of analytical tools within Cambridge Sequential Total Energy Package (CASTEP),<sup>33</sup> was used for first principles<sup>34,35</sup> calculations. The exchange correlation functional was represented by generalized gradient approximation (GGA) of the Perdew–Burke–Ernzerhof (PBE) functional.<sup>36</sup> The semi-empirical DFT-D<sub>2</sub> method of Grimmes correctly considers the weak van der Waals interaction in the material. Because the local density approximation<sup>37</sup> (LDA) generally underestimate the equilibrium atomic distances while overestimate the adsorption energy of the model system, and PBE/GGA can provide more precise estimations for geometric optimization. Therefore, the PBE/GGA were applied for geometry optimization and electronic property calculations. The cutoff energy is set as 500 eV. For both electronic and optical analyses, the convergence criterion for the self-consistent electronic loop was set to  $2 \times 10^{-6}$  eV. Simultaneously, in the

Brillouin zone, the  $3 \times 3 \times 1$  *k*-point grid is implemented for calculations. The adsorption energy<sup>38</sup> for one H atom adsorbed onto the MoSi<sub>2</sub>N<sub>4</sub> monolayer of Mo, Si, or N atom can be confirmed as

$$E_{\text{ads}} = (E_{\text{suf}} + E_{\text{H}}) - E_{\text{H-suf}} \quad (1)$$

where  $E_{\text{suf}}$ ,  $E_{\text{H}}$ , and  $E_{\text{H-suf}}$  denote the total energy of intrinsic MoSi<sub>2</sub>N<sub>4</sub>, a free H atom, and total energy of H-atom-adsorbed MoSi<sub>2</sub>N<sub>4</sub>, separately. Negative (positive) values indicates that the adsorption is an exothermic (endothermic) reaction.

The investigation focused on the thermodynamic stability of hydrogenated MoSi<sub>2</sub>N<sub>4</sub> through the computation of the formation energy ( $E_{\text{f}}$ ) using the following equation:

$$E_{\text{f}} = (E_{\text{MoSi}_2\text{N}_4\text{-H}} - mE_{\text{Mo}} - nE_{\text{Si}} - lE_{\text{N}} - kE_{\text{H}})/(m + n + l + k) \quad (2)$$

where  $E_{\text{MoSi}_2\text{N}_4\text{-H}}$ ,  $E_{\text{Mo}}$ ,  $E_{\text{Si}}$ ,  $E_{\text{H}}$  and  $E_{\text{N}}$  denote the total energies of hydrogenated MoSi<sub>2</sub>N<sub>4</sub>, the chemical potentials of Mo in the metallic bulk Mo, the chemical potentials of Si in the diamond Si, the chemical potential of H in gaseous H<sub>2</sub> molecule, and the chemical potential of N in gaseous N<sub>2</sub> molecule, respectively. The value of  $m$ ,  $n$ ,  $l$ , and  $k$  are the number of Mo, Si, N and H atoms in the system, separately.

From a quantum mechanical point of standpoint, the interaction between photons and electrons in the system is illustrated by time-dependent perturbations in the ground state, where the absorption or emission of photons causes transition between unoccupied and occupied states. The spectrum produced by excitation can be regarded as a joint density of state (DOS) between the conduction bands (CB) and the valence bands (VB). The imaginary part of the dielectric function  $\varepsilon_2(\omega)$  is a function of the photon frequency and can be described as follows:

$$\varepsilon_2(q \rightarrow Q_u, h\omega) = \frac{2\pi e^2}{\Omega \varepsilon_0} \sum_{\kappa, \nu, c} |\langle \psi_{\kappa}^c | \mu \cdot \gamma | \psi_{\nu}^c \rangle|^2 \delta(E_{\kappa}^c - E_{\nu}^c - E) \quad (3)$$

where  $k$  is the reciprocal lattice vector,  $\omega$  is the frequency of incident photon,  $u$  is the vector defining the polarization of the incident electric field, and the superscripts  $c$  and  $\nu$  denote the CB and VB, separately. The real part  $\varepsilon_1(\omega)$  of the dielectric function, since the dielectric function exhibits a causal response, can be obtained through the imaginary part of the Kramers–Kronig relations. Then the other optical spectra, such as absorption coefficient ( $\alpha(\omega)$ ), reflectivity  $R(\omega)$ , and refractivity index ( $\eta(\omega)$ ) can be gained by  $\varepsilon_1(\omega)$  and  $\varepsilon_2(\omega)$ .<sup>39–41</sup>

$$\eta(\omega) = \left[ \sqrt{\varepsilon_1^2(\omega) + \varepsilon_2^2(\omega)} - \varepsilon_1(\omega) \right]^{1/2} / \sqrt{2} \quad (4)$$

$$\alpha(\omega) = \sqrt{2}\omega \left[ \sqrt{\varepsilon_1^2(\omega) + \varepsilon_2^2(\omega)} - \varepsilon_1(\omega) \right]^{1/2} \quad (5)$$

$$R(\omega) = \left| \frac{\sqrt{\varepsilon_1(\omega) + j\varepsilon_2(\omega)} - 1}{\sqrt{\varepsilon_1(\omega) + j\varepsilon_2(\omega)} + 1} \right|^2 \quad (6)$$



### 3. Results and discussion

#### 3.1. Geometric structure of $\text{MoSi}_2\text{N}_4$ - $n\text{H}$ monolayers

Fig. 1a and b show top- and side-views of the optimized geometry structure of pristine  $\text{MoSi}_2\text{N}_4$  monolayer with the  $4 \times 4 \times 1$  supercell. The  $\text{MoSi}_2\text{N}_4$  monolayer has a hexagonal crystal symmetry with optimized lattice parameters of  $a = 2.94 \text{ \AA}$  and  $c = 20.31 \text{ \AA}$ . It has a sandwiched structure consisted of two N-Si-N layers with a Mo layer in the middle.

Next, the surface sites for H chemisorption were considered. Three different sites was computed for comparison to determine the most stable site for H chemisorption on  $\text{MoSi}_2\text{N}_4$  monolayer. Fig. 1c illustrates the chemisorption of an H on three different sites of  $\text{MoSi}_2\text{N}_4$  monolayer, referring to atop Mo, Si, and N atoms as defined as  $T_{\text{Mo}}$ ,  $T_{\text{Si}}$ , and  $T_{\text{N}}$ , respectively. Fig. 1d and e depicts top- and side-views of an H adsorbed on atop of N in  $\text{MoSi}_2\text{N}_4$  monolayer ( $\text{MoSi}_2\text{N}_4$ -1H), with the H atom adsorbed on top of an N atom.

The calculated adsorption energies of an H atop of  $T_{\text{Mo}}$ ,  $T_{\text{Si}}$  and  $T_{\text{N}}$  are  $-0.275$ ,  $-0.948$  and  $-1.601 \text{ eV}$ , respectively. The negative adsorption energies suggest that the chemisorption of H on the three sites of the  $\text{MoSi}_2\text{N}_4$  monolayer is exothermic and thermodynamically stable. Meanwhile, the lowest adsorption energy is  $-1.601 \text{ eV}$  on  $T_{\text{N}}$  site indicates it is the most stable adsorption position. Therefore, the following discussion focuses mainly on the chemisorption of different H atoms on  $T_{\text{N}}$  sites. The maximum number of H atoms adsorbed at  $T_{\text{N}}$  sites on one side of  $\text{MoSi}_2\text{N}_4$  monolayer can be estimated as 16 based on supercell size.

Then, the calculated formation energy ( $E_f$ ) for hydrogenated  $\text{MoSi}_2\text{N}_4$  was investigated to confirm the stability of

hydrogenated  $\text{MoSi}_2\text{N}_4$  further. As shown in Table 1 and Fig. S1 (ESI<sup>†</sup>), with the number of H increase, the formation energy are slightly increased because of the repulse interaction increase between the H atoms. However, the formation energy of different number of H chemisorption on the  $\text{MoSi}_2\text{N}_4$  systems are all negative, indicating the stability of the systems. This result implies the occurrence of a favorable exothermic reaction between the  $\text{MoSi}_2\text{N}_4$  monolayer and the H atom, highlighting the overall chemical stability of the structure.

Fig. 2 shows top and side view of  $\text{MoSi}_2\text{N}_4$ - $n\text{H}$ ,  $n$  is the number of H atoms adsorbed on the surface. As the number of H atoms increases, the resulting  $\text{MoSi}_2\text{N}_4$ - $n\text{H}$  retains the sandwich structure. As shown in Fig. 2d, when four H atoms are adsorbed, an adsorption energy is  $-1.69 \text{ eV}$  can be derived, which comparable to that of  $\text{MoSi}_2\text{N}_4$ -1H ( $-1.60 \text{ eV}$ ). As the number of adsorbed H atoms increases, the corresponding adsorption energy gradually becomes more negative (e.g.,

**Table 1** The calculated formation energy of the hydrogenated  $\text{MoSi}_2\text{N}_4$  monolayer system

	$E_f$ (eV)
$\text{MoSi}_2\text{N}_4$ -1H	$-1.890$
$\text{MoSi}_2\text{N}_4$ -2H	$-1.864$
$\text{MoSi}_2\text{N}_4$ -4H	$-1.823$
$\text{MoSi}_2\text{N}_4$ -6H	$-1.766$
$\text{MoSi}_2\text{N}_4$ -8H	$-1.742$
$\text{MoSi}_2\text{N}_4$ -10H	$-1.712$
$\text{MoSi}_2\text{N}_4$ -12H	$-1.683$
$\text{MoSi}_2\text{N}_4$ -14H	$-1.635$
$\text{MoSi}_2\text{N}_4$ -16H	$-1.608$
$\text{MoSi}_2\text{N}_4$ -32H	$-1.247$

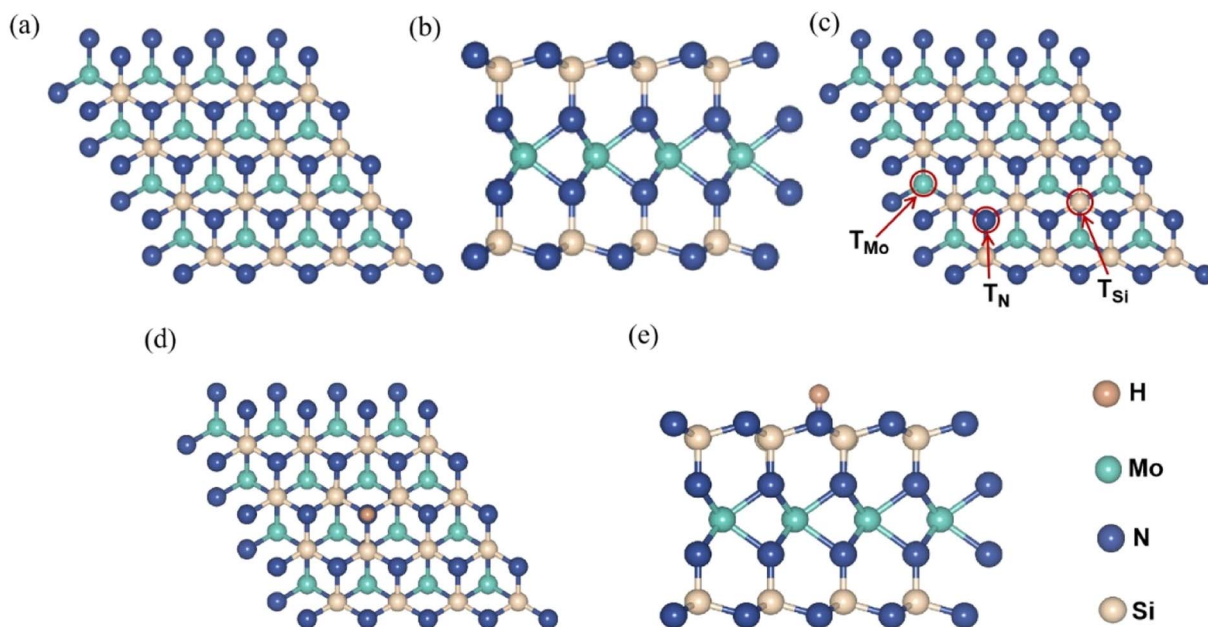


**Fig. 1** (a) and (b) top- and side-views of pristine  $\text{MoSi}_2\text{N}_4$  monolayer; (c) top view showing the different sites for chemisorption of an H atom on a  $\text{MoSi}_2\text{N}_4$  monolayer ( $T_{\text{Mo}}$ ,  $T_{\text{Si}}$ , and  $T_{\text{N}}$  represent the site atop Mo, Si, and N atoms, respectively); (d) top- and (e) side-view of a  $\text{MoSi}_2\text{N}_4$  monolayer after chemisorption of an H ( $\text{MoSi}_2\text{N}_4$ -1H).



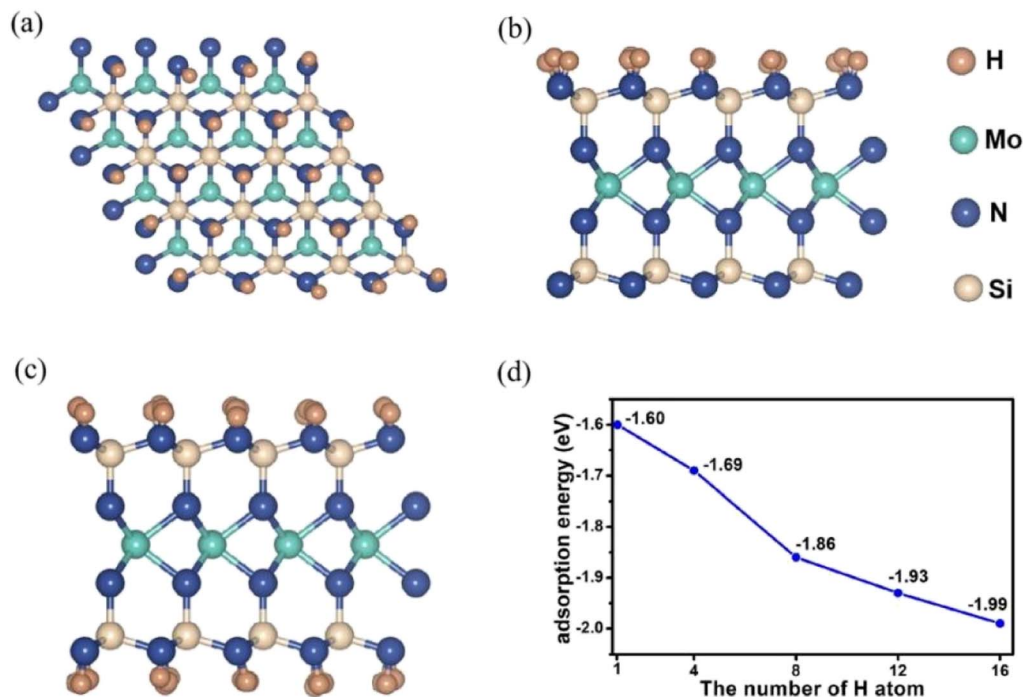


Fig. 2 (a) Top view of MoSi<sub>2</sub>N<sub>4</sub>-16H, (b) and (c) side view of MoSi<sub>2</sub>N<sub>4</sub>-16H and MoSi<sub>2</sub>N<sub>4</sub>-32H, (d) trend in the adsorption energies of MoSi<sub>2</sub>N<sub>4</sub>-*n*H (*n* = 1, 4, 8, 12, and 16).

−1.99 eV for MoSi<sub>2</sub>N<sub>4</sub>-16H). This situation illustrates that the monolayer structures remain stable with increased H atoms.

### 3.2. Electronic properties of MoSi<sub>2</sub>N<sub>4</sub>-*n*H monolayers

The effects of adsorbed H on the electronic structures of MoSi<sub>2</sub>N<sub>4</sub>-*n*H were next investigated by band structure (BS) and density of state (DOS) calculations. Fig. 3 shows the calculation results of BS and DOS of pristine MoSi<sub>2</sub>N<sub>4</sub> monolayer. The labels G, F, and H represent high-symmetry points in the Brillouin zone with fractional coordinates of G (0, 0, 0), F (0, 0.5, 0), and H (−0.333, 0.667, 0.5), respectively. The valence band maximum<sup>42</sup> (VBM) and conduction band minimum<sup>43</sup> (CBM) are located at the different positions in the G and H points of Brillouin zone, illustrating that pristine MoSi<sub>2</sub>N<sub>4</sub> is an indirect band gap semiconductor. Fig. 3a exhibits the BS of pristine MoSi<sub>2</sub>N<sub>4</sub>. The

calculated band gap is 1.89 eV, near to the experimental value of 1.94 eV.<sup>44</sup> Fig. 3b shows the computed DOS of pristine MoSi<sub>2</sub>N<sub>4</sub> monolayer. The valence band edge<sup>45</sup> (VBE) in the range of −3 to 0 eV energy level was primarily contributed by the Mo 4d and N 2p state. The conduction band edge (CBE) from 2 to 3 eV is mainly contributed by the Si 3p, Mo 4d and N 2p states.

Fig. 4 shows the calculated BS and DOS profiles of MoSi<sub>2</sub>N<sub>4</sub>-8H monolayer. Its band gap was 0.98 eV, less than that of pristine MoSi<sub>2</sub>N<sub>4</sub>. From DOS plot (Fig. 4b), its VBE in the energy range from −4 to 0 eV was primarily composed of Mo 4d and Si 3p state and CBE in the energy range from 1 to 4 eV was mainly comprised of Si 3p, Mo 4d, and H 1s state.

The band structures of the H-adsorbed MoSi<sub>2</sub>N<sub>4</sub> monolayer are shown in Fig. 5. From Fig. 5a and b, the MoSi<sub>2</sub>N<sub>4</sub>-1H and MoSi<sub>2</sub>N<sub>4</sub>-16H monolayers are both indirect semiconductors

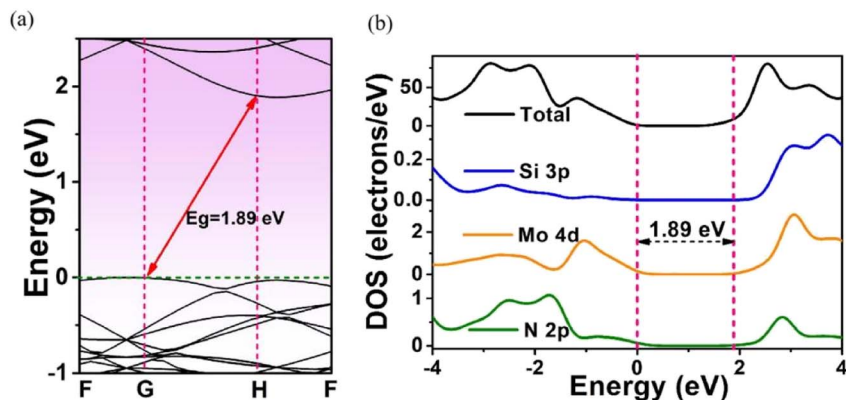


Fig. 3 (a) Energy band structure and (b) density of states (DOS) plots of a pristine MoSi<sub>2</sub>N<sub>4</sub> monolayer. The Fermi level is set at 0 eV.



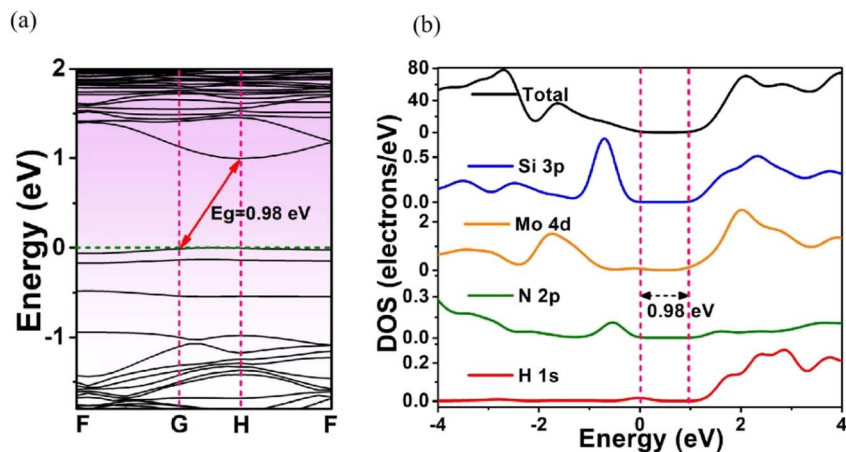


Fig. 4 (a) Energy band structure and (b) DOS of MoSi<sub>2</sub>N<sub>4</sub>-8H monolayer. The Fermi level is set at 0 eV.

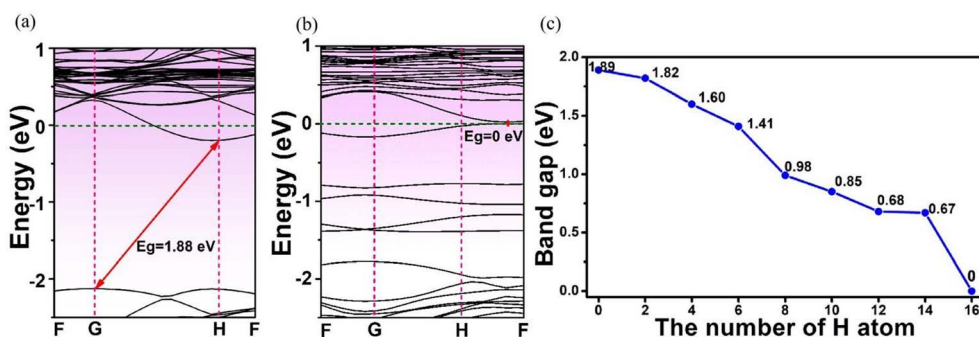


Fig. 5 Energy band structures of (a) MoSi<sub>2</sub>N<sub>4</sub>-1H and (b) MoSi<sub>2</sub>N<sub>4</sub>-16H; and (c) band gap of MoSi<sub>2</sub>N<sub>4</sub>-*n*H monolayer (*n* = 0, 2, 4, 6, 8, 10, 12, 14 and 16). MoSi<sub>2</sub>N<sub>4</sub>-*n*H denotes a MoSi<sub>2</sub>N<sub>4</sub> monolayer after chemisorption of "*n*" H atoms.

with calculated band gap values of 1.88 and 0 eV, respectively. Also, the phenomenon exhibits an indirect band gap for H-adsorbed MoSi<sub>2</sub>N<sub>4</sub>. Fig. 5c shows the band gap of the MoSi<sub>2</sub>N<sub>4</sub>-*n*H as a function of the number of H atoms ("*n*") adsorbed on MoSi<sub>2</sub>N<sub>4</sub> monolayer. It is evident that the band gap of MoSi<sub>2</sub>N<sub>4</sub>-*n*H continuously decreases as the surface-adsorbed H atom increases possibly with an increased impurity level. The decreased band gap of the MoSi<sub>2</sub>N<sub>4</sub>-*n*H monolayer suggests its

optical absorption can be extended to the visible and infrared regions properties. This enables its promising application as a potential photocatalytic material clean energy conversion and utilization.

### 3.3. Optical property variation of MoSi<sub>2</sub>N<sub>4</sub>-*n*H monolayers

The dielectric function of MoSi<sub>2</sub>N<sub>4</sub>-*n*H (*n* = 0, 1, 8 and 16) monolayers is calculated to evaluate the influence of electronic

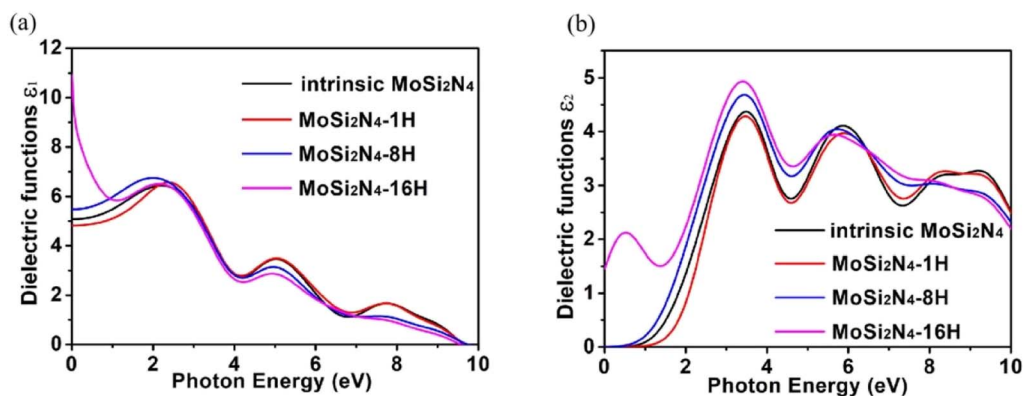


Fig. 6 Dielectric functions of the pristine MoSi<sub>2</sub>N<sub>4</sub> and MoSi<sub>2</sub>N<sub>4</sub>-*n*H (*n* = 0, 1, 8 and 16) monolayers: (a) real part; (b) imaginary part.



structure change on its optical properties (Fig. 6). Fig. 6a demonstrates the real part  $\varepsilon_1(\omega)$  of pristine and  $n$ H-adsorbed  $\text{MoSi}_2\text{N}_4$  monolayer systems. The pristine  $\text{MoSi}_2\text{N}_4$  monolayer exhibits a dielectric constant  $\varepsilon_1(0)$  of 5.1. For H atom-adsorbed  $\text{MoSi}_2\text{N}_4$  monolayer, the  $\varepsilon_1(0)$  are 4.8 (1H-chemisorption), 5.5 (4H-chemisorption) and 10.9 (16H-chemisorption), respectively. The result illustrates that  $\varepsilon_1(0)$  of the  $n$ H-adsorbed systems is significantly larger than that of the system without adsorbed hydrogen, except that of  $\text{MoSi}_2\text{N}_4$ -1H monolayer possibly due to the occasional calculation error.

A higher dielectric constant can lead to a stronger ability to bind electrons and a less polarization. Therefore, with the increase of H atom chemisorption, the polarization intensity decreases and the thermal stability of  $\text{MoSi}_2\text{N}_4$ - $n$ H system increases. Fig. 6b shows the imaginary parts of the dielectric functions. For pristine  $\text{MoSi}_2\text{N}_4$ , it can be seen that the imaginary part has three main peaks at 3.4, 6.1, and 9.1 eV, corresponding to the three intrinsic plasma frequencies. By analyzing the electronic band structure, we speculate that the peak at 3.4 eV may be caused by the electron transition between the N 2p state and the Mo 4d state in the conduction band minimum. The peaks at 6.1 and 9.1 eV may result from electronic transitions between the N 2p, Mo 4d and Si 3p states. It can also be seen that the line shapes of  $\text{MoSi}_2\text{N}_4$ - $n$ H monolayers are almost the same in all energy ranges, and the peaks of  $\text{MoSi}_2\text{N}_4$ -16H monolayer at 3.4, 6.1 and 9.1 eV are consistent with the peaks of  $\text{MoSi}_2\text{N}_4$ - $n$ H monolayer, but a weak peak is noted at 0.5 eV. However, the  $\text{MoSi}_2\text{N}_4$ -16H monolayer exhibits

a distinctly different peak shape in the 0–2 eV range. In the high energy range, the line shapes of  $\text{MoSi}_2\text{N}_4$ - $n$ H ( $n = 0, 1$  and 8), these observations indicate that the difference in the number of H atoms adsorbed mainly affect the optical properties in the low energy zone.

The absorption coefficients  $\alpha(\omega)$  of the intrinsic and H-decorated  $\text{MoSi}_2\text{N}_4$  monolayers were calculated using the obtained  $\varepsilon_1(\omega)$  and  $\varepsilon_2(\omega)$ . Fig. 7a shows the absorption spectra of pristine  $\text{MoSi}_2\text{N}_4$  and  $\text{MoSi}_2\text{N}_4$ - $n$ H monolayer. As can be seen from the figure, the absorption region becomes significantly wider after chemisorption of H, and the absorption coefficient in the visible region is greatly improved compared with the pristine  $\text{MoSi}_2\text{N}_4$ . It suggests that H chemisorption is favorable for photocatalytic activity, making  $\text{MoSi}_2\text{N}_4$ - $n$ H a potential candidate for photoelectrochemical applications.

Fig. 7b–d shows the energy-loss spectrum, that is, the reflectivity ( $R(\omega)$ ) and the refractive indices ( $n(\omega)$ ) of  $\text{MoSi}_2\text{N}_4$ - $n$ H monolayers in the range of 0–10 eV. Fig. 7b exhibits the energy loss plots, where the spike near 4.2 eV can be attributed to plasma oscillations. It is worth mentioning that the peak in the energy loss spectrum corresponds to the valleys in the reflection spectrum. It can be seen from Fig. 7c that the reflectivity drops suddenly at about 4.3 eV and keeps the same trend as the peak value of the energy loss spectrum. In the light energy range from 1.8–3.5 eV,  $\text{MoSi}_2\text{N}_4$ - $n$ H shows reflectivity peaks at 3.5 eV and refractivity peaks at 2.6 eV. The results show that H-adsorbed  $\text{MoSi}_2\text{N}_4$  has a higher refractive index and substantially unchanged reflectance in visible region.

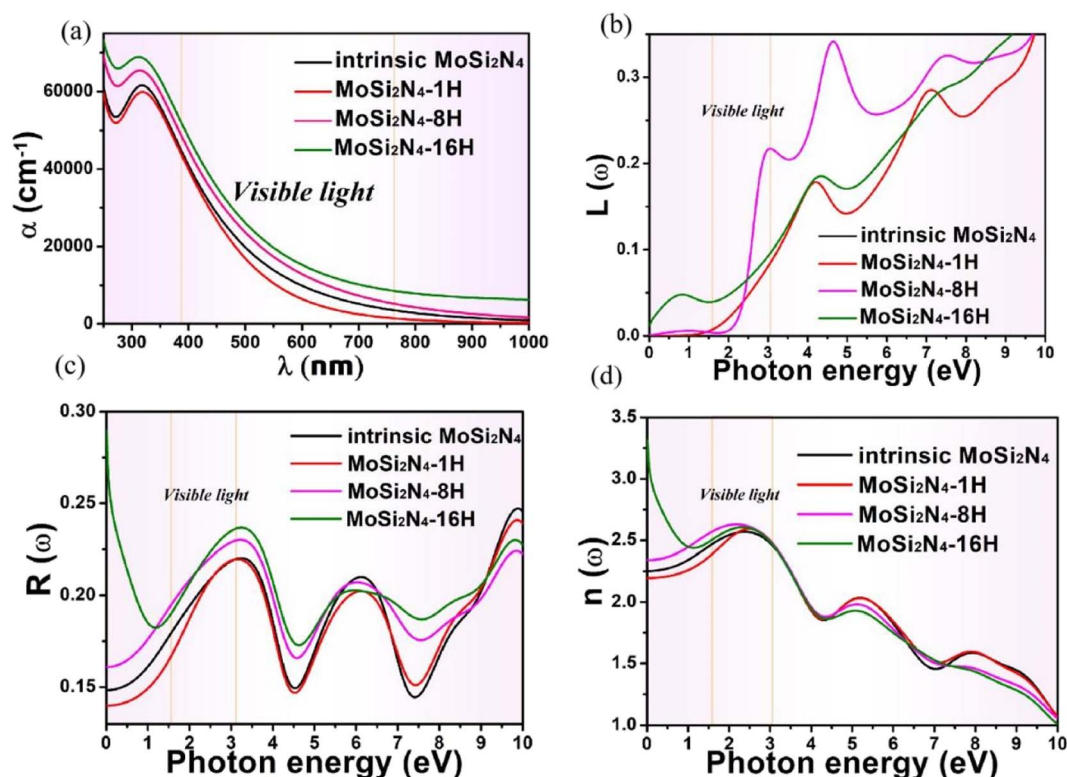


Fig. 7 (a) Absorption spectra, (b) energy loss function plots, (c) reflectivity spectra, and (d) refractivity index spectra for  $\text{MoSi}_2\text{N}_4$  and  $\text{MoSi}_2\text{N}_4$ - $n$ H ( $n = 0, 1, 8$  and 16). The pink areas indicate the visible light region.



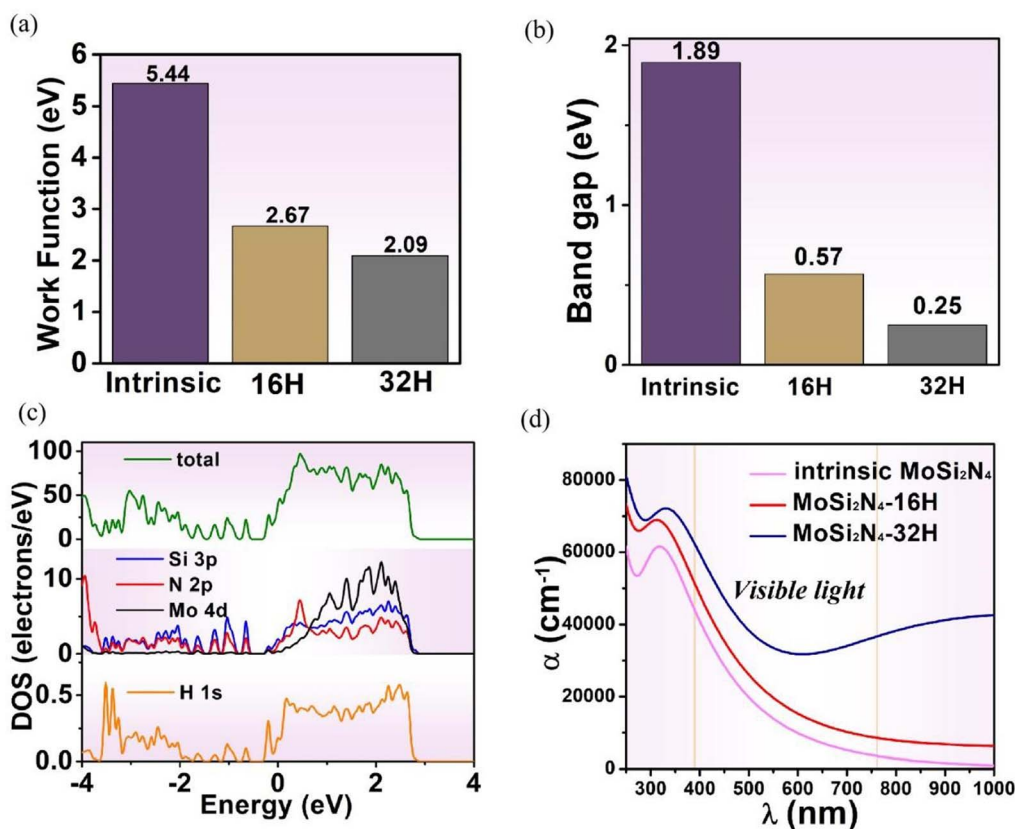


Fig. 8 (a) The change of work function  $\Phi$  for H adsorbed  $\text{MoSi}_2\text{N}_4$  systems, (b) the band gap of  $\text{MoSi}_2\text{N}_4-n\text{H}$  ( $n = 0$  and  $32$ ), (c) density of state of  $32\text{H}$ -adsorbed  $\text{MoSi}_2\text{N}_4$  monolayer, (d) absorption spectra of  $\text{MoSi}_2\text{N}_4-n\text{H}$  ( $n = 0, 16$  and  $32$ ).

### 3.4. The electronic and optical properties of semi and full-hydrogenated $\text{MoSi}_2\text{N}_4$

The work function is defined as the minimum energy for an electron escaping from the surface as can be calculated by the following equation:

$$\Phi = E_0 - E_F \quad (7)$$

where  $E_F$  and  $E_0$  are the Fermi level and the electronic potential at the vacuum level, respectively. In order to study the effect of the chemisorption of H atoms on the work function, the work functions of the pristine and adsorbed  $\text{MoSi}_2\text{N}_4$  monolayer system were calculated. Fig. 8a indicates the variation of work function after the H chemisorption on  $\text{MoSi}_2\text{N}_4$ . The calculated work functions are 5.44 and 2.09 eV for pristine and full-hydrogenated  $\text{MoSi}_2\text{N}_4$  monolayers, respectively. The change of  $\Phi$  is closely related to the change of surface conductivity, especially for monolayer. Accurate calculation of  $\Phi$  also helps to determine the direction of surface charge flow.

Fig. 8b shows the band gap variations of pristine and full-hydrogenated  $\text{MoSi}_2\text{N}_4$  systems. With the increase of the hydrogenation degree, the band gap of  $\text{MoSi}_2\text{N}_4$  monolayer system decreases continuously. The result shows that the band gap of pristine  $\text{MoSi}_2\text{N}_4$  is 1.89 eV and the full-hydrogenated  $\text{MoSi}_2\text{N}_4$  is 0.25 eV. In combination with Fig. 8c, there are two impurity energy levels of Si 3p and N 2p states, and the two

states are hybridized to form the impurity band. The impurity energy band of H 1s enters the valence band and is connected with the valence band to form a new degenerated energy band, which leads to the decrease of the gap bandwidth. The above phenomena show that hydrogenation is the main reason for the band gap decrease. Therefore, the hydrogenation can effectively modulate the size of band gap for  $\text{MoSi}_2\text{N}_4$ .

Based on the electronic property discussions, the optical properties variations of the  $\text{MoSi}_2\text{N}_4$  system are discussed. Fig. 8d depicts the absorption spectra of pristine, semi- and full-hydrogenated  $\text{MoSi}_2\text{N}_4$ , respectively. In the visible range, the absorption coefficients of full-hydrogenated  $\text{MoSi}_2\text{N}_4$  monolayers are much larger than those of the other two cases. These results indicate that full-hydrogenated  $\text{MoSi}_2\text{N}_4$  monolayer is more suitable for solar cell and photocatalytic applications.

## 4. Conclusions

In this study, the structural, electronic, and optical properties of H-adsorbed  $\text{MoSi}_2\text{N}_4$  monolayers were investigated using first principles calculations. The calculated energy of formation ( $E_f$ ) for  $\text{MoSi}_2\text{N}_4$  hydrogenation was determined to be negative, indicative of thermodynamic stability. This finding suggests the presence of a beneficial exothermic reaction between the  $\text{MoSi}_2\text{N}_4$  monolayer and the H atom, emphasizing the overall chemical stability of the structure. Also, the negative adsorption



energy indicates the stability of MoSi<sub>2</sub>N<sub>4</sub> monolayer structure adsorbed with H. The electronic structure analysis shows that the pristine MoSi<sub>2</sub>N<sub>4</sub> monolayer is an indirect band gap semiconductor (with a band gap of 1.89 eV). With the increase of H atoms adsorbed on MoSi<sub>2</sub>N<sub>4</sub> monolayer, the band gaps gradually decrease from 1.89 eV to 0 eV (16H-adsorbed) and 0.25 eV (32H-adsorbed), which indicates hydrogenation can effectively change the width of band gap and make MoSi<sub>2</sub>N<sub>4</sub> system into adjustable band-gap structure. The results of work function analysis show that H chemisorption on MoSi<sub>2</sub>N<sub>4</sub> monolayers reduces the work function value, and full-hydrogenated monolayer has a minimum work function, which is conducive to the electron transition application for photocatalysis. The optical study reveals that the chemisorption of H atoms greatly increases the dielectric constant of MoSi<sub>2</sub>N<sub>4</sub>. The visible light absorption range and visible light absorption coefficient are also increased. Moreover, compared with semi-hydrogenated chemisorption, the absorption coefficient of full-hydrogenated monolayer in the visible range is much larger. Overall, due to the unique physical and chemical properties, H-adsorbed MoSi<sub>2</sub>N<sub>4</sub> monolayers are promising candidates for novel photocatalytic materials and optoelectronic devices.

## Conflicts of interest

There are no conflicts to declare.

## Acknowledgements

This work was supported by the National Natural Science Foundation of China (no. 52262042) and Spring City Plan: The High-level Talent Promotion and Training Project of Kunming (2022SCP005).

## References

- J. Feng, M. Graf, K. Liu, D. Ovchinnikov, D. Dumcenco, M. Heiranian, V. Nandigana, N. R. Aluru, A. Kis and A. Radenovic, Single-layer MoS<sub>2</sub> nanopores as nanopower generators, *Nature*, 2016, **536**, 197–200.
- H. Li, C. Tsai, A. L. Koh, L. Cai, A. W. Contryman, A. H. Fragapane, J. Zhao, H. S. Han, H. C. Manoharan, F. Abild-Pedersen, J. K. Nørskov and X. Zheng, Activating and optimizing MoS<sub>2</sub> basal planes for hydrogen evolution through the formation of strained sulphur vacancies, *Nat. Mater.*, 2016, **15**, 48–53.
- S. B. Desai, S. R. Madhvapathy, A. B. Sachid, J. P. Llinas, Q. X. Wang, G. H. Ahn, G. Pitner, M. J. Kim, J. Bokor, C. M. Hu, H. S. P. Wong and A. Javey, MoS<sub>2</sub> transistors with 1-nanometer gate lengths, *Science*, 2016, **354**, 99–102.
- Y. L. Hong, Z. B. Liu, L. Wang, T. Y. Zhou, W. Ma, C. Xu, S. Feng, L. Chen, M. L. Chen, D. M. Sun, X. Q. Chen, H. M. Cheng and W. C. Ren, Chemical vapor deposition of layered two-dimensional MoSi<sub>2</sub>N<sub>4</sub> materials, *Science*, 2020, **369**, 670.
- W. Shi, G. Yin, S. Yu, T. Hu, X. Wang and Z. Wang, Atomic precision tailoring of two-dimensional MoSi<sub>2</sub>N<sub>4</sub> as electrocatalyst for hydrogen evolution reaction, *J. Mater. Sci.*, 2022, **57**, 18535–18548.
- J. Q. Ng, Q. Wu, L. K. Ang and Y. S. Ang, Tunable electronic properties and band alignments of MoSi<sub>2</sub>N<sub>4</sub>/GaN and MoSi<sub>2</sub>N<sub>4</sub>/ZnO van der Waals heterostructures, *Appl. Phys. Lett.*, 2022, **120**, 103101.
- C. Q. Nguyen, Y. S. Ang, S.-T. Nguyen, N. V. Hoang, N. M. Hung and C. V. Nguyen, Tunable type-II band alignment and electronic structure of C<sub>3</sub>N<sub>4</sub> MoSi<sub>2</sub>N<sub>4</sub> heterostructure: interlayer coupling and electric field, *Phys. Rev. B*, 2022, **105**, 045303.
- C. V. Nguyen, C. Q. Nguyen, S. T. Nguyen, Y. S. Ang and N. V. Hieu, Two-Dimensional Metal/Semiconductor Contact in a Janus MoSH/MoSi<sub>2</sub>N<sub>4</sub> van der Waals Heterostructure, *J. Phys. Chem. Lett.*, 2022, **13**, 2576–2582.
- X. H. Xu, L. Yang, Q. Gao, X. X. Jiang, D. M. Li, B. Cui and D. S. Liu, Type-II MoSi<sub>2</sub>N<sub>4</sub>/MoS<sub>2</sub> van der Waals Heterostructure with Excellent Optoelectronic Performance and Tunable Electronic Properties, *J. Phys. Chem. C*, 2023, **127**, 7878–7886.
- Z. Cui, K. Yang, K. Ren, S. Zhang and L. Wang, Adsorption of metal atoms on MoSi<sub>2</sub>N<sub>4</sub> monolayer: a first principles study, *Mater. Sci. Semicond. Process.*, 2022, **152**, 107072.
- Z. Cui, Y. Luo, J. Yu and Y. Xu, Tuning the electronic properties of MoSi<sub>2</sub>N<sub>4</sub> by molecular doping: a first principles investigation, *Phys. E*, 2021, **134**, 114873.
- A. Castellanos-Gomez, X. Duan, Z. Fei, H. R. Gutierrez, Y. Huang, X. Huang, J. Quereda, Q. Qian, E. Sutter and P. Sutter, Van der Waals heterostructures, *Nat. Rev. Methods Primers*, 2022, **2**, 58.
- W. Zhou, X. Zhou, C. Yang, J. Zhang, L. Wang and Q. Li, Tunable type-II lateral MoSi<sub>2</sub>N<sub>4</sub>/WSi<sub>2</sub>N<sub>4</sub> heterostructures for photocatalytic applications, *Phys. Chem. Chem. Phys.*, 2022, **24**, 26307–26315.
- M. L. Sun, Q. Q. Ren, Y. M. Zhao, J. P. Chou, J. Yu and W. C. Tang, Electronic and magnetic properties of 4d series transition metal substituted graphene: a first-principles study, *Carbon*, 2017, **120**, 265–273.
- M. L. Sun, W. C. Tang, Q. Q. Ren, Y. M. Zhao, S. K. Wang, J. Yu, Y. H. Du and Y. T. Hao, Electronic and magnetic behaviors of graphene with 5d series transition metal atom substitutions: a first-principles study, *Phys. E*, 2016, **80**, 142–148.
- Y. Luo, S. K. Wang, S. H. Li, Z. M. Sun, J. Yu, W. C. Tang and M. L. Sun, Transition metal doped puckered arsenene: magnetic properties and potential as a catalyst, *Phys. E*, 2019, **108**, 153–159.
- S. Wang and J. Yu, Magnetic Behaviors of 3d Transition Metal-Doped Silicene: a First-Principle Study, *J. Supercond. Novel Magn.*, 2018, **31**, 2789–2795.
- M. Sun, Q. Ren, S. Wang, Y. Zhang, Y. Du, J. Yu and W. Tang, Magnetism in transition-metal-doped germanene: a first-principles study, *Comput. Mater. Sci.*, 2016, **118**, 112–116.
- M. Sun, Q. Ren, Y. Zhao, S. Wang, J. Yu and W. Tang, Magnetism in transition metal-substituted germanene: a search for room temperature spintronic devices, *J. Appl. Phys.*, 2016, **119**, 143904.



- 20 S. K. Wang, H. Y. Tian, Y. Luo, J. Yu, C. D. Ren, C. L. Sun, Y. J. Xu and M. L. Sun, First-principles calculations of aluminium nitride monolayer with chemical functionalization, *Appl. Surf. Sci.*, 2019, **481**, 1549–1553.
- 21 M. Sun, J.-P. Chou, Y. Zhao, J. Yu and W. Tang, Weak C–H···F–C hydrogen bonds make a big difference in graphane/fluorographane and fluorographene/fluorographane bilayers, *Phys. Chem. Chem. Phys.*, 2017, **19**, 28127–28132.
- 22 W. Tang, M. Sun, Q. Ren, S. Wang and J. Yu, Halogenated arsenenes as Dirac materials, *Appl. Surf. Sci.*, 2016, **376**, 286–289.
- 23 W. Tang, M. Sun, Q. Ren, Y. Zhang, S. Wang and J. Yu, First principles study of silicene symmetrically and asymmetrically functionalized with halogen atoms, *RSC Adv.*, 2016, **6**, 95846–95854.
- 24 M. Sun, Q. Ren, S. Wang, J. Yu and W. Tang, Electronic properties of Janus silicene: new direct band gap semiconductors, *J. Phys. D: Appl. Phys.*, 2016, **49**, 445305.
- 25 T. V. Vu, N. T. T. Anh, D. M. Hoat, D. P. Tran, H. D. Tong, H. L. Luong, L. M. Hieu, C. V. Nguyen, H. V. Phuc, N. T. T. Binh and N. N. Hieu, Electronic, optical and photocatalytic properties of fully hydrogenated GeC monolayer, *Phys. E*, 2020, **117**, 113857.
- 26 T. V. Vu, K. D. Pham, T. N. Pham, D. D. Vo, P. T. Dang, C. V. Nguyen, H. V. Phuc, N. T. T. Binh, D. M. Hoat and N. N. Hieu, First-principles prediction of chemically functionalized InN monolayers: electronic and optical properties, *RSC Adv.*, 2020, **10**, 10731–10739.
- 27 R. Chen, D. Chen and W. Zhang, First-principles calculations to investigate stability, electronic and optical properties of fluorinated MoSi<sub>2</sub>N<sub>4</sub> monolayer, *Results Phys.*, 2021, **30**, 104864.
- 28 H. Liu, B. Huang, Y. Dai and W. Wei, Characteristic excitonic absorption of MoSi<sub>2</sub>N<sub>4</sub> and WSi<sub>2</sub>N<sub>4</sub> monolayers, *J. Phys. D: Appl. Phys.*, 2023, **56**, 405103.
- 29 M. D. Segall, J. D. L. Philip, M. J. Probert, C. J. Pickard, P. J. Hasnip, S. J. Clark and M. C. Payne, First-principles simulation: ideas, illustrations and the CASTEP code, *J. Phys.: Condens. Matter*, 2002, **14**, 2717.
- 30 H. G. Si, Y. X. Wang, Y. L. Yan and G. B. Zhang, Structural, Electronic, and Thermoelectric Properties of InSe Nanotubes: First-Principles Calculations, *J. Phys. Chem. C*, 2012, **116**, 3956–3961.
- 31 Y. Xiao, C. Shen and W. B. Zhang, Screening and prediction of metal-doped  $\alpha$ -borophene monolayer for nitric oxide elimination, *Mater. Today Chem.*, 2022, **25**, 100958.
- 32 C. Zhang, F. Wei, X. Zhang, W. Chen, C. Chen, J. Hao and B. Jia, Thermoelectric properties of monolayer MoSi<sub>2</sub>N<sub>4</sub> and MoGe<sub>2</sub>N<sub>4</sub> with large Seebeck coefficient and high carrier mobility: a first principles study, *J. Solid State Chem.*, 2022, **315**, 123447.
- 33 W. Zhang, W. Yang, Y. Liu, Z. Liu and F. Zhang, Computational exploration and screening of novel Janus MA<sub>2</sub>Z<sub>4</sub> (M = Sc–Zn, Y–Ag, Hf–Au; A = Si, Ge; Z = N, P) monolayers and potential application as a photocatalyst, *Front. Phys.*, 2022, **17**, 63509.
- 34 R. S. Uwanyuze, S. P. Alpay, S. Schaffner and S. Sahoo, A first principles analysis of oxidation in titanium alloys with aluminum and vanadium, *Surf. Sci.*, 2022, **719**, 122026.
- 35 C. Rebolledo Espinoza, D. A. Ryndyk, A. Dianat, R. Gutierrez and G. Cuniberti, First principles study of field effect device through van der Waals and lateral heterostructures of graphene, phosphorene and graphane, *Nano Mater. Sci.*, 2022, **4**, 52–59.
- 36 N. Mwanemwa, H.-E. Wang, T. Zhu, Q. Fan, F. Zhang and W. Zhang, First principles calculations investigation of optoelectronic properties and photocatalytic CO<sub>2</sub> reduction of (MoSi<sub>2</sub>N<sub>4</sub>)<sub>5–n</sub>/(MoSiGeN<sub>4</sub>)<sub>n</sub> in-plane heterostructures, *Results Phys.*, 2022, **37**, 105549.
- 37 M. T. Entwistle, M. J. P. Hodgson, J. Wetherell, B. Longstaff, J. D. Ramsden and R. W. Godby, Local density approximations from finite systems, *Phys. Rev. B*, 2016, **94**, 205134.
- 38 J. C. Tracy, Structural Influences on Adsorption Energy. II. CO on Ni(100), *J. Chem. Phys.*, 2003, **56**, 2736–2747.
- 39 A.-M. Hu, L.-L. Wang, W.-Z. Xiao and B. Meng, Electronic structures and magnetic properties in Cu-doped two-dimensional dichalcogenides, *Phys. E*, 2015, **73**, 69–75.
- 40 H. Belhadji, M. Ameri, B. Abbar, N. Moulay, A. Z. Bouyakoub, O. Arbouche, D. Bensaid, I. Ameri, S. Mesbah and Y. Al-Douri, Optical properties of (Pb<sub>1–x</sub>Mn<sub>x</sub>S)<sub>1–y</sub>Fe<sub>y</sub> materials from first-principles calculations, *Chin. J. Phys.*, 2017, **55**, 1032–1043.
- 41 K. Boudiaf, A. Bouhemadou, O. Boudrifa, K. Haddadi, F. S. Saoud, R. Khenata, Y. Al-Douri, S. Bin-Omran and M. A. Ghebouli, Structural, Elastic, Electronic and Optical Properties of LaOAgS-Type Silver Fluoride Chalcogenides: First-Principles Study, *J. Electron. Mater.*, 2017, **46**, 4539–4556.
- 42 S.-C. Liu, C.-M. Dai, Y. Min, Y. Hou, A. H. Proppe, Y. Zhou, C. Chen, S. Chen, J. Tang, D.-J. Xue, E. H. Sargent and J.-S. Hu, An antibonding valence band maximum enables defect-tolerant and stable GeSe photovoltaics, *Nat. Commun.*, 2021, **12**, 670.
- 43 H. Mizoguchi, S.-W. Park, T. Katase, J. Yu, J. Wang and H. Hosono, Unique Conduction Band Minimum of Semiconductors Possessing a Zincblende-Type Framework, *Inorg. Chem.*, 2022, **61**, 10359–10364.
- 44 J. Yu, J. Zhou, X. Wan and Q. Li, High intrinsic lattice thermal conductivity in monolayer MoSi<sub>2</sub>N<sub>4</sub>, *New J. Phys.*, 2021, **23**, 033005.
- 45 D. J. Trainer, A. V. Putilov, C. Di Giorgio, T. Saari, B. K. Wang, M. Wolak, R. U. Chandrasena, C. Lane, T. R. Chang, H. T. Jeng, H. Lin, F. Kronast, A. X. Gray, X. X. Xi, J. Nieminen, A. Bansil and M. Iavarone, Inter-Layer Coupling Induced Valence Band Edge Shift in Mono-to Few-Layer MoS<sub>2</sub>, *Sci. Rep.*, 2017, **7**, 42619.